RESEARCH PAPER

Development of Porous Character in Tamarind Wood-Derived Charcoal by Microwave-Assisted Sodium Chloride Activation for Methylene Blue Adsorption

Sumrit Mopoung*, Khachidapron Seeoon

* *sumritm@nu.ac.th*

Chemistry Department, Faculty of Science, Naresuan University, Phitsanulok, Thailand, 65000

Received: July 2024 **Revised: April 2025** **Accepted: May 2025**
DOI: 10.22068/ijmse.3647

Abstract: *Activated carbon preparation from tamarind wood-derived charcoal by microwave-assisted sodium chloride activation was studied to investigate the effects of 0-5 wt.% NaCl and 450-850 W microwave heating power. The properties of the derived products were analyzed by FTIR, XRD, SEM-EDS, and BET. Methylene blue adsorption by the activated carbon products was also studied to evaluate the contract time, pH, methylene blue concentration, and adsorption isotherms. The study's results showed that the percent yields (77.42-92.52%) of the fabricated activated carbons decrease with increasing wt.% of NaCl and MP. On the other hand, the contents of disordered graphitic carbon, carbonate, basic surface functional groups, and mesopores increased. However, 3 wt.% NaCl and 600 W microwave irradiation power were identified as appropriate conditions for activation, which created the micro-mesopore (pore size range 1.59-14.76 nm) on the surface of the derived activated carbon products. Optimal values of equilibrium time and pH for methylene blue adsorption are 60 minutes and 8, respectively. The results of methylene blue concentrations were fitted to the Langmuir isotherm indicating 33.33 mg/g as the maximum methylene blue adsorption capacity.*

Keywords: *Tamarind wood charcoal, Activated carbon, Microwave irradiation, Sodium chloride, Methylene blue.*

1. INTRODUCTION

Microwave-assisted irradiation is one of the advanced techniques that have caught researchers' attention for the production of activated carbon [1]. This is because it has many advantages such as improved heat distribution uniformity, shorter processing times, higher heating efficiencies, low degree of hazardous by-products, quick internal heating [2], excellent control of the reaction parameters, selective heating, if the reaction mixture contains compounds with different microwave absorbing properties, higher yields, better selectivity due to reduced side reactions, improved reproducibility, automatization and high throughput synthesis, and reasonable control of shape and size [3]. Therefore, activated carbon preparation by microwave-assisted chemical activation is a low-cost and straightforward process [4] as the starting material effectively absorbs electromagnetic radiation. Microwave heating for chemically activated carbon preparation can be generated from either dipole polarization or ionic conduction. Carbon-based materials, which act as microwave energy absorbers, are suitable for microwave-heating due to the delocalized π electrons from sp^2-hybridized carbon networks. Collisions of the movement of electrons in carbon networks with atomic ions generate the heating. The heating is also generated by interfacial polarization, which causes friction and heat from rotating electron dipoles [5]. Alternatively, microwaves can also heat ionic activator via oscillating collisions of charged species under an alternating electromagnetic irradiation of 0.001–1.000 m wavelength and 0.3–300 GHz frequency [3], which is conducted by dipolar polarization and ionic conduction When a microwave is applied, the dipoles rotate with a delay to the change of the electric field, which causes friction and heat. The movement of charged ions can generate heat by collisions with neighboring molecules or atoms [5]. Energy conversion from microwave into heat energy depends upon the interaction of the electric and magnetic field components with the material during irradiation [3]. Accordingly, carbon-based materials mixed with ionic solutions can be adopted to improve microwave energy conversion efficiency and facilitate heating [3]. Chemical agents used together with microwave heating for activation during activated carbon preparation include $ZnCl_2$ [2], KOH [6], K_2CO_3 [7], and NaOH/KOH mixture [8]. For biomass starting

[Downloaded from survey.iust.ac.ir on 2025-07-27]

[DOI: 10.22068/ijmse.3647]

materials, microwave-assisted chemical activation has been used for activated carbon preparation from blue coke powder [6], carrot juice pulp, and pomegranate peel [2]. The present research uses tamarind wood (TW) as a precursor of a charcoal product made using a traditional method. TW is a low-cost waste rich in lignocellulosic materials with a carbon content of around 40-50% [9]. It has been used for activated carbon preparation employing either $ZnCl_2$ and activation at 439°C [10], or H_3PO_4 and activation at 800°C [9]. NaCl has also been considered as an activator in combination with microwaves for activated carbon production. Sodium chloride is a neutral activation agent.

It has been used for activated carbon preparation by the conventional heating method from palm oil palm [11] and sunflower seed shells [12]. However, it has not been used for activation in combination with microwave heating. To evaluate the potential application of the activated carbon product fabricated in this research, methylene blue (MB) was used for an adsorption study. MB is one of the most widely used dyes in the large-scale dyeing process, which has been dumped into aquatic ecosystems that directly affect human health and aquatic ecosystems [13]. MB contains a basic group in its structure and dissociates in water to produce positive ions with a diameter of about 0.8-0.9 nm. It is often used to assess the adsorption capacity of adsorbents for organic-like pollutants [6]. MB can cause cyanosis, jaundice, tissue necrosis, methemoglobinemia, and quadriplegia. In addition, it is carcinogenic and mutagenic to humans. MB also disrupts the growth of plants as it merges with phosphate and lipid molecules in plants' cell membranes [14].

Therefore, this research aims to study the development of porosity in tamarind wood-derived charcoal (TWC) prepared using microwave-assisted sodium chloride activation for MB removal. The primary purpose of this work is to simplify the method of activating charcoal production from TW waste. The properties of the derived product were analyzed by FTIR, XRD, SEM-EDS, and BET. Moreover, the adsorption behavior of MB on the fabricated tamarind wood-derived activated charcoal (TWAC) in terms of equilibrium time, the effects of pH, MB concentration, and adsorption isotherms were investigated.

2. EXPERIMENTAL PROCEDURES

2.1. Preparation of Charcoal

The TW was obtained from Phetchabun Province, Thailand. It was sun-dried for 2 weeks and cut into pieces 5 cm long. The dried wood pieces (10 kg) were loaded in tubular earthenware pot with a lid and placed in an electric furnace (Fisher Scientific Isotemp® Muffle Furnace, Pennsylvania, USA) for carbonization for 1h at 450°C and then cooled to room temperature. The percent yield of the charcoal product was then calculated. The derived charcoal was kept in a desiccator for further analysis and experiments.

2.2. Preparation of Activated Charcoal

Samples (10 g) of the fabricated charcoal were impregnated with 0, 1.0, 3.0, and 5.0 wt.% NaCl (99.5%, Merck company) solutions. The mixed samples were suspended in 10 mL distilled water for mixing, dissolving, and then dried in an oven (SL 1375 SHEL LAB 1350 FX, Oregon, USA) at 100°C overnight. The dried mixtures were activated in a microwave-assisted heating chamber (SAMSUNG ME711K, 20 L, Bangkok, Thailand) at microwave irradiation power of 450 W, 600 W, or 850 W for 10 minutes. The percent yields of the final products were calculated. The fabricated TWACs were ground, sieved to 80 mesh (Laboratory test sieve, Retsch, Germany), and kept in a desiccator for further analysis and experiments.

2.3. Characterization of Charcoals and Activated Charcoals

The fabricated TWC and TWACs were characterized by FTIR (Spectrum GX, Perkin Elmer, Connecticut, USA), XRD (PW 3040/60, X' Pert Pro Console, Philips, Netherland), SEM-EDS (Leo1455VP Electron Microscopy, Cambridge, England), and BET (Micromeritics TriStar II3020, Bavaria, Germany). Finally, the TWACs with the best characteristics were used for MB adsorption experiments in order to determine the equilibrium time, optimum pH, initial concentration, and isotherm adsorption type.

2.4. Methylene Blue Adsorption

The effects of different parameters such as contact time, pH, and concentration of MB were investigated. Langmuir and Freundlich isotherm models were also fitted to the experimental equilibrium data.

[Downloaded from survey.iust.ac.ir on 2025-07-27]

[DOI: 10.22068/ijmse.3647]

2.4.1. Equilibrium time of methylene blue adsorption

A100 mg/L stock solution of MB (AR UNILAB) was prepared by dissolving 0.1 g of MB powder in 1 L of deionized water. Batch experiments were used for MB adsorption. A 0.1000 g (Analytical balance; Sartorius ED224s Germany) sample of the TWAC was added into an Erlenmeyer flask containing 25 mL of 10 mg/L MB solution at pH 7.0±0.15 (Mettler Toledo) and then shaken continuously at 120 rpm and a temperature of 32±2ºC with contact times of 20, 40, 60, 80, 100, 120, 140, 160, and 180 minutes. The supernatant solutions (1 mL) were pipetted and then diluted with 100 mL, pH 7 buffer solution KH_2PO_4 (CARLO ERBA Reagent) and Na_2HPO_4 (Ajax Finechem). These solutions were then filtered using a Whatman no. 42 filter paper to remove the TWAC particles as reach of each contact time. The absorbance values of the resulting MB blue filtrates were measured at 665 nm using UV/Visible spectrometer (UNICO 1100, Georgia, USA). The concentrations of the MB filtrate solutions were calculated from the absorbance values using a standard calibration curve. The data from this experiment was plotted to determine the equilibrium time.

2.4.2. The effect of pH on methylene blue adsorption

The effect of pH was studied under conditions like the investigation of equilibrium time with 60 min contact time at pH values of 2, 3, 4, 5, 6, 7, 8, and 9, respectively. A sample of 0.1000 g of the TWAC was added to an Erlenmeyer flask containing 25 mL of 10 mg/L MB solution at pH 7.0±0.15 and then shaken continuously at 120 rpm and a temperature of 32±2ºC. The pH values of the solutions were adjusted with 0.05 M HCl (reagent grade, Merck) or NaOH solution (reagent grade, Merck). Then, MB concentration in the filtrates from all experiments was measured.

2.4.3. The effect of methylene blue concentration

The batch adsorption experiments for studying the effect of MB concentration were carried out with a fixed dose of TWACs of 0.10 g. Experiments were carried out with 60 min contact time at a pH of 8.0 with MB concentrations of 50 mg/L, 75 mg/L, 100 mg/L, 125 mg/L, 150 mg/L, and 200 mg/L. Accurately weighed samples (0.10 g) of TWACs were placed into an Erlenmeyer flask and mixed with MB at the selected concentration. The MB concentration in the filtrates from each experiment was measured.

2.4.4. Adsorption isotherms

The data from the MB adsorption experiment were fitted with both the linear form of the Langmuir equation [Eq. (1)] and the Freundlich equation [Eq. (2)] as follows:

The linear form of the Langmuir equation is [15]:

$$C_e/Q_e = 1/(q_{max}K_L) + C_e/q_{max} \quad (1)$$

Where: Q_e (mg/g) is the amount of MB adsorbed per unit mass of TWAC. Ce (mg/L) is the MB equilibrium concentration. Q_{max} (mg/g) is the maximum MB amount that forms a complete monolayer on the surface of the TWAC. K_L (L/mg) is the Langmuir constant, which is associated with adsorption heat. The constants Q_{max} and K_L were determined from the slope and intercept of a plot of C_e/Q_e versus C_e, respectively. The Langmuir model could be estimated by a dimensionless separation factor, which indicates whether the sorption is favorable or not. The separation factor, R_L is defined as [16]:

$$R_L = 1/(1+K_L C_0) \quad (2)$$

where C_0 (mg/L) is the initial concentration of MB, K_L (L/mg) is the Langmuir constant. Values of $0< R_L< 1$ indicate that the sorption is favorable. The linear form of the Freundlich equation is [15]:

$$LogQ_e = LogK_F + (1/n)LogC_e \quad (3)$$

Q_e and C_e have the same definitions as those in the Langmuir equation cited above. K_F and n are Freundlich constants related to adsorption capacity and heterogeneity factor, respectively. The constants K_F and n can be determined from the intercept and slope of a plot of Log C_e against Log Q_e, respectively.

3. RESULTS AND DISCUSSION

3.1. Percent Yield of TWC and TWACs

The percent yield of TWC, which was carbonized at 450°C, is quite high (40.28%), because it is a hard wood with 40-50% carbon content [9]. After the activation process, the percent yields (Figs. 1a-c), based on the TWC as a starting material, of the TWACs decrease with increasing microwave irradiation power from 450 W to 850 W and wt.% of NaCl from 0% to 5%. Considering the effects of microwave power (MP) (0 wt.% NaCl and 450-850 W), these

[Downloaded from survey.iust.ac.ir on 2025-07-27]

[DOI: 10.22068/ijmse.3647]

results indicate increasing amounts of microwave radiation being absorbed by the TWC in response to increasing MP. As a result, dipole rotations of the carbon atoms within the charcoal matrix were induced to a high frequency and generated high amounts of heat energy [8]. These very rapid rotations of the carbon atoms within the TWC matrices improved the pyrolysis cracking of the TWC and released more volatile matter. Therefore, lower yields of TWACs were obtained due to the release of more volatile matter from the char, which then transformed into the TWACs, with increasing texture characteristics of the TWAC [17]. For the effect of 1-5 wt.% NaCl and 450-850 W, the increasing amounts of hydrated Na^+ and Cl^- ions, which were trapped in the carbon structure of TWC matrices, induced a high degree of swelling [11]. This could weaken the surface structure of the TWC by dehydration reactions and then result in increased carbon burning [11] to volatile substances (e.g. CH_4, CO_2, or CO), along with the development of a microporous structure or the enlargement of micropores into mesopores on the activated carbon products [8]. As an additional consideration, the amount of energy (KJ) provided by microwave irradiation can be estimated with Eq. (4) [8].

Energy (KJ)= [W×time (s)]/1000 (4)

where W is the microwave irradiation power, and the irradiation time is in seconds.

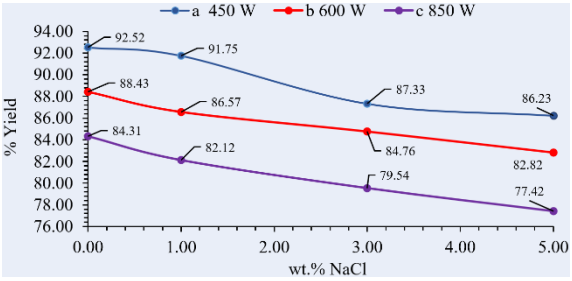

Fig. 1. Percent yield of TWACs with 0-5.00 wt.% NaCl and MP of a) 450 W, b) 600 W, and c) 800 W

The calculated energies are 270 KJ, 360 KJ, and 510 KJ for MP of 450 W, 600 W, and 850 W, respectively. Therefore, carbon-carbon single bonds (bond energy= 350 KJ) [8] in the TWC could be broken down at 600 W to 850 W of MP. On the other hand, carbon-=carbon double bonds (bond energy= 600 KJ) [8] cannot be destroyed with 600 W to 850 W and 600 s of irradiation time. Therefore, the percent yields of the activated carbon products are high for microwave irradiation between 450 W to 850 W. At the same time, the carbon atoms in the charcoal matrix are removed due to combustion at high concentrations of NaCl. This is due to the TWC matrices being seeped, coated, and protected from heat by NaCl [11]. However, the addition of NaCl activator also caused the degradation of some remaining organic material in TWC weakening the surface structure and then causing the release of volatile substances and development of microporous structure on the TWACs [11]. Furthermore, the percent yields of activated carbons without NaCl addition are higher than yields obtained with 1-3 wt.% NaCl addition for the same MP. This is because there is no reaction between the NaCl activator and the carbon surface. In addition, it was observed that the decreases in the percent yields of TWACs with increasing of wt.% NaCl are relatively lower than the yield decreases observed in response to the increase of MP. This is attributed to the formation of carbonate by NaCl, while the effect of MP mediates no carbonate formation.

3.2. XRD of TWC and TWACs

The XRD patterns of TWCs showed two wide bands at 2θ values of about 24° and 44.5°, which are associated with the disordered graphitic and graphitic planes, respectively (Fig. 2a). This is the background of carbon materials, which exhibit high porosity [12]. This shows that TW was transformed into TWC by the carbonization process at 450°C. The TWACs also exhibited the disordered graphitic and graphitic planes (Figs. 2b-e). However, the bands at 2θ of about 24° for TWACs, which is characteristic of disordered graphitic or a low graphitization of the TWAC sample [9], become more intense with increasing wt.% of NaCl from 1% to 5% (shown only at 600 W). This was attributed to the depolymerization of aromatic structure units and was accelerated by NaCl to produce more volatiles and smaller aromatic structures [18]. At the same time, the disordered graphitic phase of the products is also augmented by increasing MP from 450 W to 850 W (Figs. 3a-c, shown only at 3 wt.% NaCl). This confirms that the MP and NaCl concentrations both affected the porosity development in the products. This could be explained by the fact that the delocalized pi-electrons in the graphitic region of the charcoal material would absorb more microwave energy

[Downloaded from survey.iust.ac.ir on 2025-07-27]

[DOI: 10.22068/ijmse.3647]

with increasing MP and collide more with atomic ions [5]. Simultaneously, the hydrated Na^+ ions in NaCl ionic liquid were also induced and generated heat by collisions [5]. These hydrated Na^+ ions could collide with neighboring high energy carbon atoms. As a result, disordered graphitic phase content in the TWACs increased. At the same time, more Na_2CO_3 was formed with increasing MP and wt.% of NaCl. The main component of the TWACs and TWCs is Na_2CO_3 (Figs. 2a-e and Figs. 3a-c). The XRD patterns of Na_2CO_3 in all products are like those in the report by Zhu et al. [19]. The more Na_2CO_3 content formed from the dehydration reactions of NaCl and carbon [12] as follows:

$$3H_2O + C + 2NaCl \rightarrow Na_2CO_3 + 2H_2 + 2HCl \quad (5)$$

Furthermore, metallic sodium could have played a role in catalyzing gasification by the following reactions [12]:

$$2NaCl + H_2O \rightarrow Na_2O + 2HCl \quad (6)$$

$$Na_2O + C \rightarrow 2Na + CO \quad (7)$$

$$2Na + H_2O \rightarrow Na_2O + H_2 \quad (8)$$

$$Na_2O + CO_2 \rightarrow Na_2CO_3 \quad (9)$$

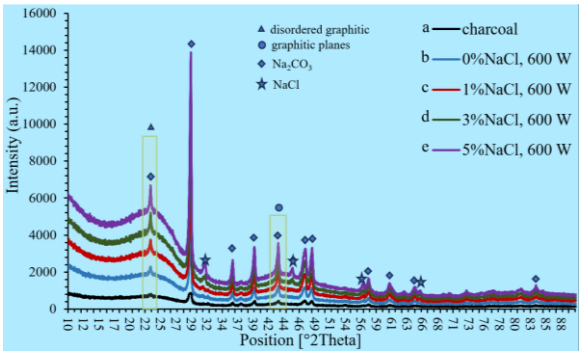

Fig. 2. XRD patterns of a) TWC, b) TWAC made with 0 wt.% NaCl and 600 W, c) TWAC made with 1 wt.% NaCl and 600 W, d) TWAC made with 3 wt.% NaCl and 600 W, and e) TWAC made with 5 wt.% NaCl and 600 W

The porosity of the TWAC is developed by these reactions (Eqs. 5-9) during the activation process. Furthermore, the peaks corresponding to Na_2CO_3 exhibit increasing intensity in response to increasing MP and NaCl concentration. This is because the reactions of sodium and surface carbon are more extensive at higher values of MP and NaCl concentration. Moreover, some Na_2CO_3 have also formed in the TWC. In this case, it has formed due to the Na content of the original TW precursor. However, a small amount of NaCl remained in the TWACs as ≥3 wt.% of NaCl. This was confirmed with XRD patterns (Figs. 2e and d), which exhibit the corresponding peaks at 31.62°, 45.3°, 56.4°, and 66.2° [20].

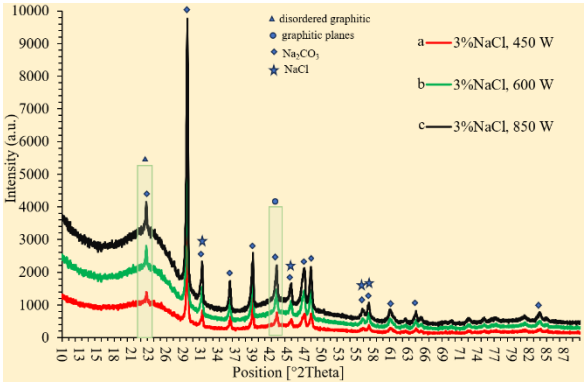

Fig. 3. XRD patterns of a) TWAC made with 3 wt.% NaCl and 450 W, b) TWAC with 3 wt.% NaCl and 600 W, and c) TWAC made with 3 wt.% NaCl and 850 W

3.3. FTIR of TWC and TWAC

The FTIR spectra of the TWC and TWACs made with 0 wt.% to 5 wt.% of NaCl and activation using 600 W are shown in Fig. 4 (the figure shows results only for MP at 600 W). These results show that carbonate is the main basic surface functional group on the TWACs (Figs. 4b-e) with corresponding peaks located at 3500 cm^{-1}-3600 cm^{-1}, 2303 cm^{-1}, 2134 cm^{-1}, 1415 cm^{-1}, 837 cm^{-1}, 819 cm^{-1}, 740 cm^{-1}, 713 cm^{-1}, and 559 cm^{-1}. These peaks or bands of carbonate correspond to the data reported by Zhu et al. [19]. This data is also in accord with the observed XRD patterns. Furthermore, the spectra include a peak with strong intensity at 1415 cm^{-1}, which corresponds to C=C bonds of graphitic carbon formed by NaCl activation. This observation is consistent with the reports of Bahiraei and Behin [12] and Maulina et al. [11]. The result could be explained by the polarization of C=C bonds of hexagonal rings through interacting with oxygen atoms (from C=O or carbonate) near one of the C atoms [21]. However, this peak decreases with increasing wt.% of NaCl used for activation. This confirms the increasing amorphous characteristics of the TWACs observed in the XRD patterns. Other basic surface functional groups are C=O (2134 cm^{-1}, 1800-1900 cm^{-1}, and 1415 cm^{-1}) [11], C-O, and COOH (1135 cm^{-1}, and 1028 cm^{-1}) [10], which are formed during carbonization and activation. Furthermore, Si-O (819 cm^{-1}) and Si-O-Si (417 cm^{-1})

[Downloaded from survey.iust.ac.ir on 2025-07-27]

[DOI: 10.22068/ijmse.3647]

groups [22], which are from the precursors, are observed in the products. In addition, the OH groups of metal hydroxide with low intensities are located at 3550 cm^{-1}-3700 cm^{-1} (Na-OH, K-OH, Ca-OH) [23, 24], 3744 cm^{-1} (Si-OH) [25], and Mg-OH [26]. These components have also originated from the precursors. Furthermore, a peak observed at 3867 cm^{-1} is attributed to the OH stretching of alcohol [27], which also formed during the activation. The CO groups, which have a basic nature, can resist temperatures as high as 950°C and are not eliminated during the microwave treatment [17]. It was seen that the surface functional groups on the TWACs have basic properties. This is because oxygen containing surface acidic functional groups are more weakly attached to the carbon surface than basic ones, and are decomposed and released as CO_2 and CO [17] by heat from microwave irradiation. Therefore, the TWACs are composed mainly of amorphous carbon structures with different basic surface groups containing oxygen, which have a profound effect on the surface characteristics of the TWACs and thus affect their adsorption properties.

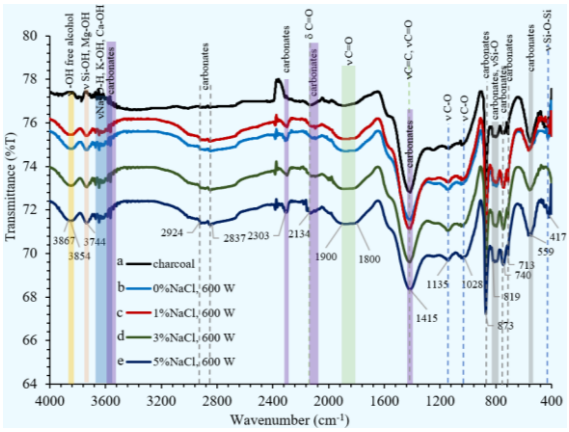

Fig. 4. FTIR transmission spectra of a) TWC, b) TWAC made with 0 wt.% NaCl and 600 W, c) TWAC made with 1 wt.% NaCl and 600 W, d) TWAC made with 3 wt.% NaCl and 600 W, and e) TWAC made with 5 wt.% NaCl and 600 W

In addition, the basic properties of the TWAC could be attributed to the delocalized π-electrons of the basal planes, which would be reinforced when surface oxygen functional groups are removed from the TWAC surface [17]. Moreover, the TWC intermediate showed the same characteristics as the TWACs (Fig. 4a) with corresponding XRD patterns. Considering the effect of MP (Figs. 5a-c), it was revealed that the characteristics of the TWACs were likely affected by it as well as by the effect of increasing wt.% of NaCl as evidenced by the XRD patterns.

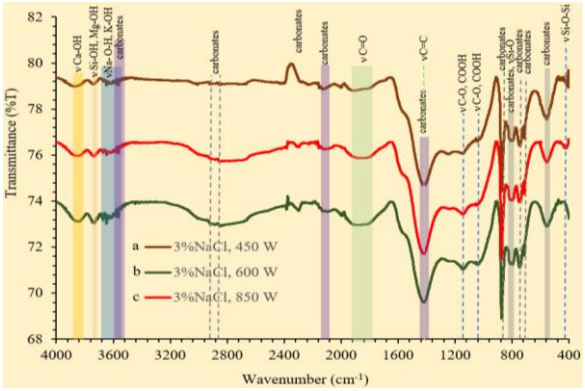

Fig. 5. FTIR transmission of a) TWAC made with 3 wt.% NaCl and 450 W, b) TWAC made with 3 wt.% NaCl and 600 W, and c) TWAC made with 3 wt.% NaCl and 850 W

3.4. Surface Morphology

The surface morphologies of the TWC and TWACs are presented in Fig. 6. It was found that macro hole channels have formed in all the products. These channels are the original xylem and phloem of the wood texture. Numerous small particles are observed on the surface of the TWC (Fig. 6a). The content of these particles decreases with an increasing wt.% of NaCl and MP (Figs. 6b-m). This is attributed to the sodium cation (Na^+), which, in combination with high heat energy, can act as a catalyst for the decomposition of small particles into volatile matters [18]. Focusing on the surface of all the products, it was found that they exhibit a high content of small pores, a rough and hard texture, and cracks on the surface. These characteristics are caused by attacks of high energy Na^+ ions onto the carbon structures of the TWC during activation [11]. However, some particles have accumulated on the TWAC surfaces. These particles are sodium carbonate and sodium chloride, remaining after the activation process.

3.5. Element Composition from EDS

Table 1 shows the elemental composition of the TWC and TWACs determined using EDS with limit detection at one decimal place. Therefore, if the content of an element is less than 0.1 wt.%, its content cannot be determined by EDS and the corresponding value is not shown.

[Downloaded from survey.iust.ac.ir on 2025-07-27]

[DOI: 10.22068/ijmse.3647]

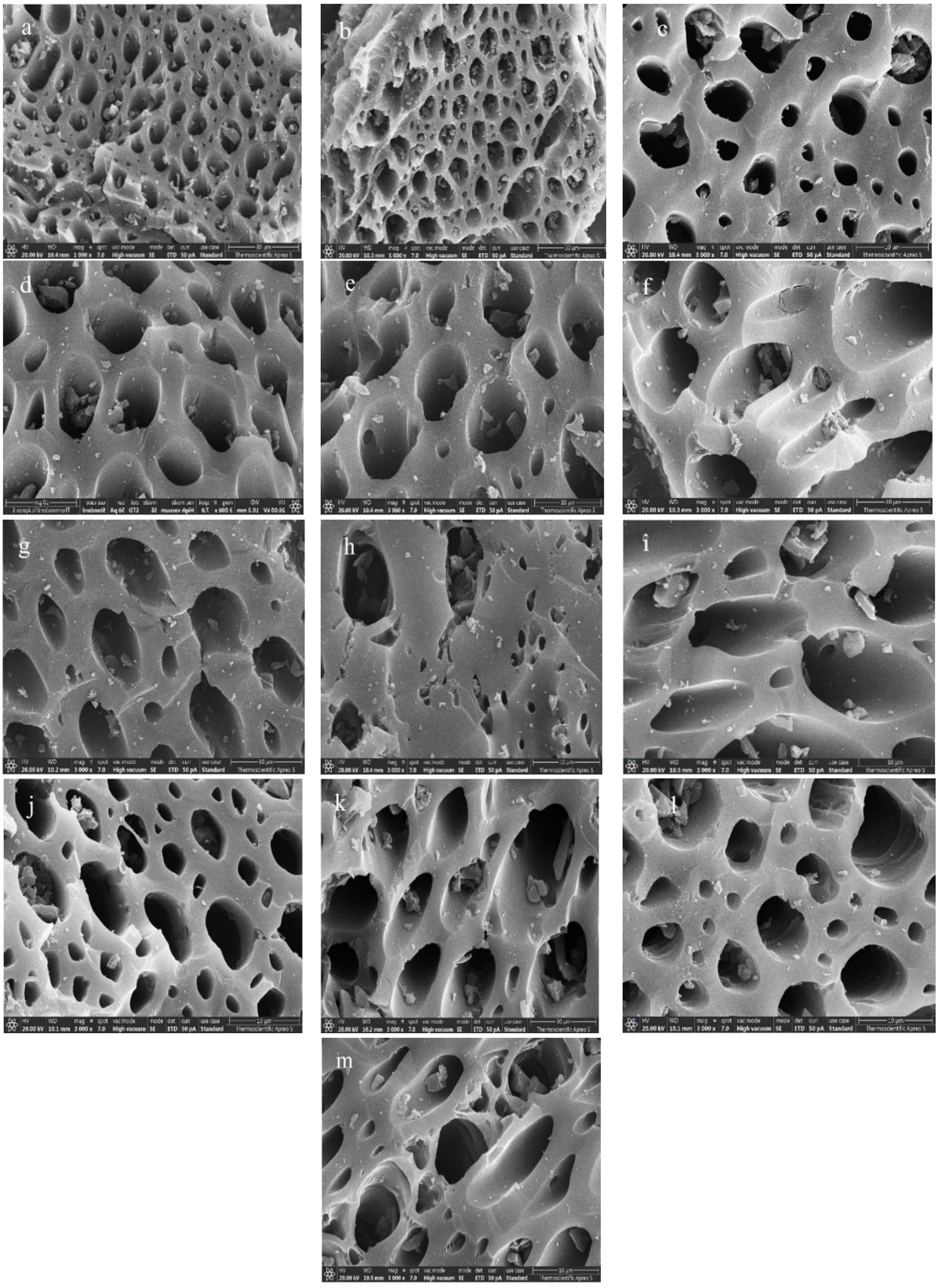

Fig. 6. SEM images of TWC a), and TWAC made with 0 wt.% NaCl and 450 W b), with 1 wt.% NaCl and 450 W c), with 3 wt.% NaCl and 450 W d), with 5 wt.% NaCl and 450 W e), with 0 wt.% NaCl and 600 W f), with 1 wt.% NaCl and 600 W g), with 3 wt.% NaCl and 600 W h), with 5 wt.% NaCl and 600 W i), with 0 wt.% NaCl and 850 W j), with 1 wt.% NaCl and 850 W k), with 3 wt.% NaCl and 850 W l), and with 5 wt.% NaCl and 850 W (m)

[Downloaded from survey.iust.ac.ir on 2025-07-27]

[DOI: 10.22068/ijmse.3647]

Table 1. Elemental composition of TWC and TWACs

Samples	Elements Composition (wt.%)							
	C	O	Ca	Mg	Na	Cl	K	Si
Charcoal	89.3	10.4						
AC 0% NaCl, 450 W	90.0	9.9						
AC 1% NaCl, 450 W	93.2	6.4						
AC 3% NaCl, 450 W	92.3	7.2			0.1	0.1		
AC 5% NaCl, 450 W	93.3	7.5			0.1	0.1		
AC 0% NaCl, 600 W	91.5	7.1						
AC 1% NaCl, 600 W	94.7	5.3						
AC 3% NaCl, 600 W	93.3	6.2			0.2	0.1		
AC 5% NaCl, 600 W	93.4	6.4			0.2	0.2		
AC 0% NaCl, 850 W	92.9	7.0	1.0	0.2				
AC 1% NaCl, 850 W	87.9	8.7	1.0	0.2				0.1
AC 3% NaCl, 850 W	92.4	6.4	1.3	0.2	0.2	0.1	0.1	0.2
AC 5% NaCl, 850 W	92.8	6.2	1.5	0.2	0.2	0.2	0.2	0.2

Consequently, content values for elements such as Ca, Mg, K, Si, Na, and Cl are not shown for some products, as the content was less than 0.1 wt.%. However, the values for the content of these elements were possible to be determined at high wt.% of NaCl and MP. This is due to the high decomposition of volatile matters and carbon content of TWC during intensive activation. When considering these results, the carbon content of the charcoal derived from hard TW is also high after 450°C carbonization temperature. However, high oxygen content has remained with a low content of some metals and Si (contained in raw TW). This result corresponds to the FITR results, which show relatively high intensities of oxygen containing surface functional groups (Fig. 4). Furthermore, the Na element is also present in the TWC. Therefore, a small amount of carbonate could be formed by the reaction of Na and surface carbon atoms during carbonization. For TWACs, the carbon content shows an increasing trend, while oxygen content shows a decreasing trend with increasing MP from 450 W to 850 W (for 0 wt.% NaCl). This was attributed to acidic surface oxygen functional groups on the TWC surface being released as CO_2 and CO during the activation process only at 450 W [17]. However, these changes are relatively low, especially as MP increases from 600 W to 850 W. This is because only the acidic oxygen containing surface functional groups were completely removed during the microwave treatment at 450 W, while basic oxygen containing surface functional groups, especially CO groups, can resist temperatures as high as 950°C and are not eliminated during the microwave treatment [17]. Therefore, the oxygen content of the TWACs is constant in the MP range of 600 to 850 W. Furthermore, a small amount of Na and Cl elements remained in the TWACs made with 3-5 wt.% of NaCl after microwave treatment. This shows that a large amount of Na and Cl are released as volatiles during the activation with microwave irradiation. This result corresponds to the XRD patterns (Figs. 2e and d). This is because the melting point and boiling of NaCl are 801°C and 1465°C, respectively [28]. Furthermore, the formation of some Na containing intermediates (such as -O-Na and −COONa) was observed, which can fix Na within the TWAC [29]. Moreover, the dehydration reaction of NaCl and surface carbon, and catalyzing gasification of Na metal and surface carbon on TWC surface produced Na_2CO_3 after the activation process. The small amount of remaining NaCl and some $NaCO_3$ produced during the activation are accumulated on the surface of the TWACs, which was confirmed by XRD and SEM results.

3.6. Surface Area and Porosity of TWC and TWACs

The BET surface area, micropore volume, pore volume and average pore size of TWC are 94.59 (m^2/g), 0.052 cm^3/g, 0.73 cm^3/g and 1.64 nm, respectively. These characteristics promote the diffusion of activating agents into the interior of the TWC structure and aid in the formation of active sites during the activation [18]. For the TWACs, the BET surface area, pore volume, micropore content, and average pore size increase with increasing wt.% of NaCl and MP (Figs. 7A-D). This could be explained by the MP increases in more microwave irradiation is delivered to the

[Downloaded from survey.iust.ac.ir on 2025-07-27]

[DOI: 10.22068/ijmse.3647]

materials and induces the generation of greater amount of heat energy within the NaCl impregnated TWC matrix leading to a sharp temperature rise. At the same time, the heat energy could be absorbed by the hydrated Na^+ and Cl^- ions from the TWC matrix. These highly energetic ions exhibiting high rotation can create new micropores and enlarge micropores into mesopores on the surface of the TWAC via intercalation and gasification reactions during the activation process. Therefore, the total pore volume [Figs. 7C(a-c)] and pore size [Figs. 7D(a-c)] of the TWACs are increased. This is due to the insertion or migration of highly energized Na^+ ions into the carbon structure of the impregnated TWC matrix during the intercalation resulting in the formation of new micropores or mesopores on the surface and thus leading to an increase of the surface area [Figs 7A(a-c)] and total pore volume of the TWACs [8]. As the pore volume of the TWAC is increased, the surface area is also increased. This shows that the activation process occurred on the surface of the carbon particles [30] because microwave radiation can only penetrate the carbon texture on a micro-scale [5]. This also affected the mean size of the pores with increasing wt.% of NaCl and MP [Figs. 7D(a-c)]. Although the diameter of the hydrated Na^+ ion is only 0.720 nm [31], the pore widths of the pores on TWACs are in the range between 0.823 and 2.52 nm [Figs. 7D(a-c)]. This could be explained that the highly energetic hydrated sodium ions, which received heat energy from microwave radiation, exhibit more vigorous motions (e.g. translational motion and rotational motion) on the TWC surface and migrated more extensively into the carbon structure of the TWC. As a result, mesopores or micropores of the TWACs were created [8] with a larger pore width than the diameter of hydrated Na^+ ions. At the same time, the sodium metal atoms produced from the reduction by carbon can reach the carbon structure, which has also created some new pores and widening of the micropores into mesopores [12].

In addition, more extensive decomposition of carbon to volatile matter is observed with increasing wt.% of NaCl loading, leading to the relatively more developed pore structure and surface area of TWACs by depolymerization and cross-linking recombination of aromatic structures [18]. However, the diameter [Figs. 7D(a-c)] and the volume of the pores [Figs. 7C(a-c)] increase slightly with increasing MP. This is due to TWC experiencing high temperature with a sharp rise, which causes the contraction of carbon skeleton and shrinking in pore structure of micropores, mesopores, and pores of different width [17]. Therefore, increasing the MP has little effect on the average pore width and pore volume.

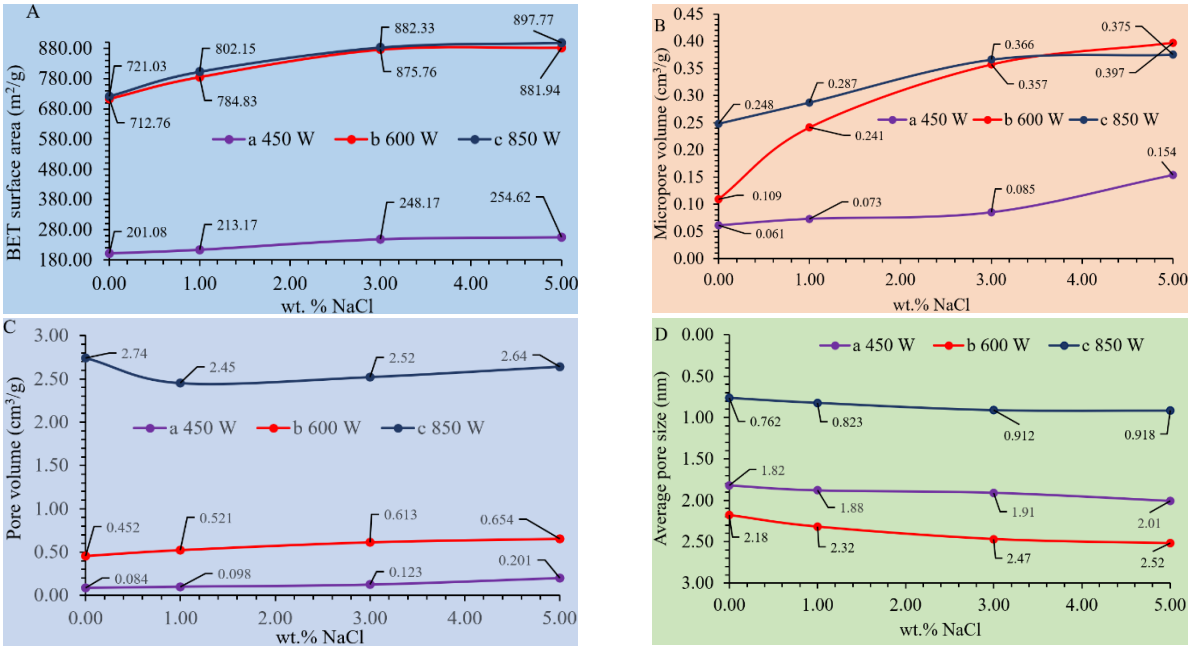

Fig. 7. Porosity characteristics of TWACs: A) BET surface area, B) micropore volume, C) pore volume, and D) average pore size with 0-5.00 wt.% NaCl and MP of a) 450 W, b) 600 W, and c) 850 W

[Downloaded from survey.iust.ac.ir on 2025-07-27]

[DOI: 10.22068/ijmse.3647]

Furthermore, the pore volume and surface area increase with increasing wt.% of NaCl from 3% to 5% and MP from 600 W to 850 W. This was attributed to the formation of many small particulate materials blocking the pores of TWC and undesired reactions taking place at excessive reaction temperatures due to extreme heating rate of high MP [5], and the release of too much volatile matter at high wt.% of NaCl loading. Moreover, the higher content of carbonated basic surface functional groups has contributed to the reorganization of aromatic fragments, leading to the relatively developed pore structure [18].

Therefore, the TWAC exhibiting hierarchical structure (micropore and mesopore) and basic oxygen containing surface functional groups made using activation with 3 wt.% of NaCl and 650 W activation was collected for further MB adsorption experiments. The pore width distribution data of TWAC prepared using activation with 3 wt.% of NaCl and 600 W, which was determined by the BJH method, is shown in Fig. 8. The pore size distribution curves show that the pore widths fall within a range between 1.59 and 14.76 nm with BET average pore width of 2.47 nm. This indicates that most of the pores exhibit mesoporous structures. Therefore, this TWAC may possess high adsorption capacity for MB with easy diffusion into the mesoporous carbon and adsorption on the pore surface [32].

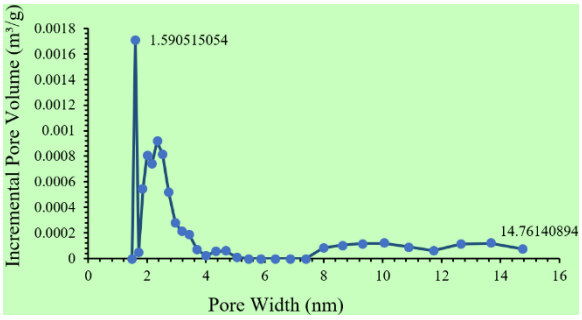

Fig. 8. Pore width distribution of TWAC made using activation with 3 wt.% of NaCl and 600 W determined by the BJH method

3.7. Methylene Blue Adsorption

The different tendencies of adsorption efficiencies of adsorbate and adsorbent can be attributed to porosity and surface area, as well as to the surface functional groups on the adsorbent that play critical roles in the physisorption and chemisorption progression [1]. MB ($C_{16}H_{18}ClN_3S$, Molecular weight of 319.86 g/mol) is found in many textile industrial effluents. It can cause severe health problems for the public and the environmental ecology [33]. It is the potential cause of cyanosis, jaundice, tissue necrosis, methemoglobinemia, quadriplegia, and it is carcinogenic and mutagenic for humans. MB can also disrupt the growth of plants as it merges with phosphate and lipid molecules in plants' cell membranes [14]. It is used to evaluate the removal capacity of porous carbon materials and others [34]. The MB molecule has a diameter of 1.447 nm [35]. However, it can only enter larger micropores and mesopores [36]. It is protonated in water, which produces positive ions, and can bind to the negatively charged active sites of activated carbon through electrostatic attraction or hydrogen bonding [37]. Therefore, the removal of MB blue by activated carbon is mainly through chemical adsorption [38]. Important factors, which influence the adsorption performance of adsorbents are contact time, pH, and adsorption isotherm [33]. Therefore, these factors were the focus for MB adsorption experiments described below.

3.7.1. Effect of contact time

The TWAC was made using 3 wt.% of NaCl, and 600 W was collected for MB adsorption experiments. The MB removal (%) is a function of the adsorption time. This was investigated using the collected activated carbon product for various adsorption times (0-180 minutes), and the results are shown in Fig. 9. Rapid adsorption is observed in the first 20 min of contact time, followed by a more gradual adsorption rate in the contact time range of 20-60 min. The results show that the equilibrium was achieved at 60 min of contract time. The rapid initial stage of the adsorption process is due to the high MB concentration gradient, providing significant driving forces towards adsorption sites [39], and the availability of an initial large number of vacant surface-active sites on the TWAC, which attracted the MB by electrostatic force [40]. At the equilibrium stage, the filling of the originally vacant sites becomes saturated, which leads to repulsive forces between the adsorbed MB molecules on the TWAC surface and MB molecules from solution [41]. The percentage of MB removed after reaching equilibrium ranges between 96.36% and 97.74%. This high percentage of MB removal is attributed to the high content

[Downloaded from survey.iust.ac.ir on 2025-07-27]

[DOI: 10.22068/ijmse.3647]

of basic surface functional groups providing electrostatic attractions and porous structure for easy transfer of MB from aqueous solutions via macropores to mesopores and micropores. Therefore, 60 min contact time was set for further MB adsorption experiments.

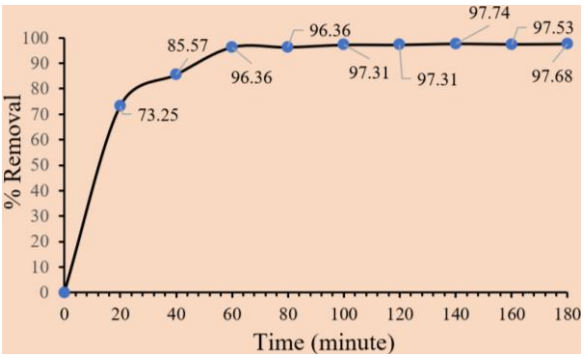

Fig. 9. Adsorption equilibrium time with contact time of 0-180 minutes for TWAC made with 3 wt.% of NaCl and 600 W

3.7.2. The effect of pH on methylene blue removal efficiency

Figure 10 shows the effect of pH on the percentage of MB removed from the solution. It can be seen that increasing pH results in an increase in the percentage of MB removed up to pH 8. Decreases in MB removal percentage are observed for pH values above 8. This could be explained by the lower removal percent of MB at low pH values due to the presence of H^+ ions competing with the cationic groups on the MB for active adsorption sites [42]. At the same time, the number of positively charged sites on the TWAC is high while the number of negatively charged sites is low. Therefore, the electrostatic repulsion between the active sites (basic surface functional groups: carbonyl, carbonate units and aromatic rings) on the surface and the positively charged MB inhibits the adsorption mechanism pathway [43]. As pH values increase, the content of negatively charged functional group sites on the TWAC surface increases due to deprotonation [44]. This favors the electrostatic attraction between the positively charged MB and the TWAC [40]. This is attributed to the pK_a (5.6) [35] of the MB. MB is not dissociated at pH values lower than 5.6 and dissociates to a cation which can interact with negatively charged surfaces at pH values higher than 5.6. The electrostatic repulsion between the positively charged MB and the positively charged surface of the TWAC is lowered as surface charge density decreases with an increase in solution pH. Therefore, the high removal of MB observed at fundamental pH values corresponds to results reported by El-Bery et al. [34]. These results are attributed to the basic surface functional groups (especially carbonate) present on the TWAC, which was confirmed by the FTIR and XRD data. However, the maximum MB removal (96.36%) was achieved at pH 8 and it then decreased after pH 8. This was attributed to the increase in electrostatic attraction and the decrease of acid effect for the coordination bonds stability between the electropositive MB and basic surface functional groups [45] at pH 8. After pH 8, it is attributed to the excess OH^- ions in the environment forming a complex with the cationic MB, which reduces adsorption due to the low effect of electrostatic adsorption [46]. Therefore, pH 8 was selected for the experiment exploring the effect of MB concentration.

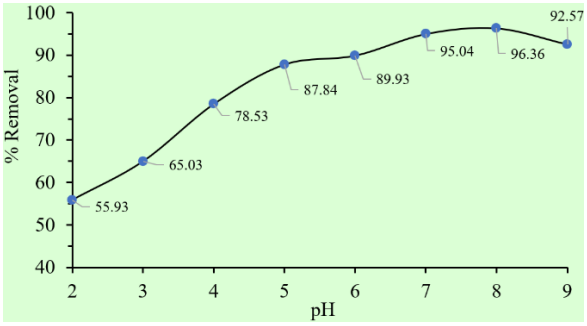

Fig. 10. Effect of the pH (2-9) values on percent removal of MB after 60 min contract time by TWAC made with 3 wt.% of NaCl and 600 W

3.7.3. Effect of initial methylene blue concentration

The effect of the initial MB concentration on the TWAC (Qe) is shown in Fig. 11. The curve indicates that the Qe values increase with increasing initial MB concentration. A gradually increasing value of Qe is observed between 50 and 125 mg/L of the initial MB concentration. The rate of increase of adsorbed MB slows down after 125 mg/L of the initial MB concentration. These results were attributed to the increase of driving force of MB molecules due to the concentration gradient, which resulted in a higher number of collisions between surface active sites on the TWAC and MB molecules [47]. This

[Downloaded from survey.iust.ac.ir on 2025-07-27]

[DOI: 10.22068/ijmse.3647]

phenomenon could increase the chance of bonding between the positively charged MB ions and negatively charged surface active sites on the TWAC by electrostatic attraction. Thus, the MB adsorption capacities by the TWAC were gradually increased for initial methylene concentrations of 50 mg/L-125 mg/L. This indicates that the saturation of negatively charged surface active sites on the TWAC is almost reached. After that, the abundance of the remaining unoccupied active sites on the TWAC surface is low for binding with positively charged MB ions at initial MB concentrations >125 mg/L. However, the Qe values increase for initial MB concentrations >125 mg/L. This is due to the high initial MB concentration providing a high driving force to overcome all mass transfer resistance [48], with attraction increasing on the remaining unoccupied active sites of the TWAC surface. Considering the curve's trend, it may be predicted that the surface binding sites on the TWAC are saturated at 200 mg/L of initial MB concentration. In the next step, the calculated values of Ce, Qe, Ce/Qe, Log Ce, and Log Qe (Table 2) are further used to study the MB adsorption isotherm.

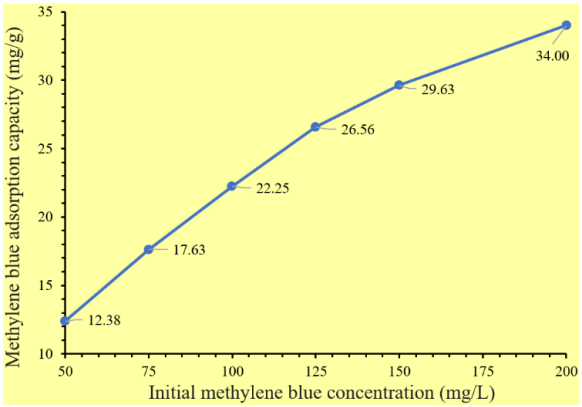

Fig. 11. Effect of initial MB concentration on MB adsorption capacity by TWAC

3.7.4. Methylene blue adsorption isotherm

The MB adsorption isotherm results indicate that the Langmuir isotherm (Fig. 12a) fits the experimental data better than the Freundlich isotherm (Fig. 12b), based on the values of the respective coefficients of determination (R^2). This has revealed that the adsorption process is based on monolayer adsorption and mostly occurs on the surface-active sites by electrostatic interaction [49] of MB and the TWAC. The MB adsorption occurred on a homogeneous surface with no interaction and transmigration in the plane of the neighboring surface [21]. The values of R_L are in the range between 0.0212 and 0.0797 (Table 3), which is between 0 and 1. This indicates homogeneity of the adsorbents and favorable adsorption [41]. It is assumed that each adsorption active site is equal, and that the filling of an adsorption site does not affect adsorption on adjacent sites [50]. However, the K_L value of 0.2308 L/mg is indicative of weak binding between MB and the TWAC, which results in reversibility of the adsorption process [33]. This phenomenon is attributed to the main fraction of the carbonate species at pH 8, HCO_3^-. The CO_3^{2-} form of carbonate appears pH 8 and becomes dominant at pH 12 [51]. Therefore, the binding energy between MB and HCO_3^- on the TWAC surface is relatively weak. Based on the Langmuir model, the maximum MB adsorption capacity of the TWAC is 33.33 mg/g (Table 3), corresponding to the Qe value observed at an initial MB concentration of 200 mg/L (Table 2). This confirmed the trend for saturation of the surface binding sites on the TWAC at 200 mg/L of initial MB concentration. A comparison with other activated carbon materials indicates that this maximum adsorption capacity TWAC made by activation with NaCl and microwave irradiation is higher than for palm kernel shell-derived activated carbon (14.7 mg/g) made by steam activation [50], and close to capsicum straw derived activated carbon (34.12 mg/g) made by KOH activation [41] with conventional heating activation.

Table 2. Calculate parameters of initial methylene blue concentration effect

Initial Concentration (mg/L)	C_e (mg/L)	Q_e (mg/g)	Ce/Q_e	Log C_e	Log Q_e
50	0.50	12.375	0.0404	-0.3010	1.0925
75	4.50	17.625	0.2553	0.6532	1.2461
100	11.00	22.250	0.4944	1.0414	1.3473
125	18.75	26.563	0.7059	1.2730	1.4243
150	31.50	29.625	1.0633	1.4983	1.4717
200	64.00	34.000	1.8824	1.8062	1.5315

[Downloaded from survey.iust.ac.ir on 2025-07-27]

[DOI: 10.22068/ijmse.3647]

Table 3. Summary of the Langmuir and Freundlich isotherm parameters calculated from the adsorption process

Langmuir Model			Freundlich Model		
Q_{max} (mg/g)	K_L (L/mg)	R_L	K_F	1/n	n
33.3333	0.2308	0.0212-0.0797	13.759416	0.2146	4.6598

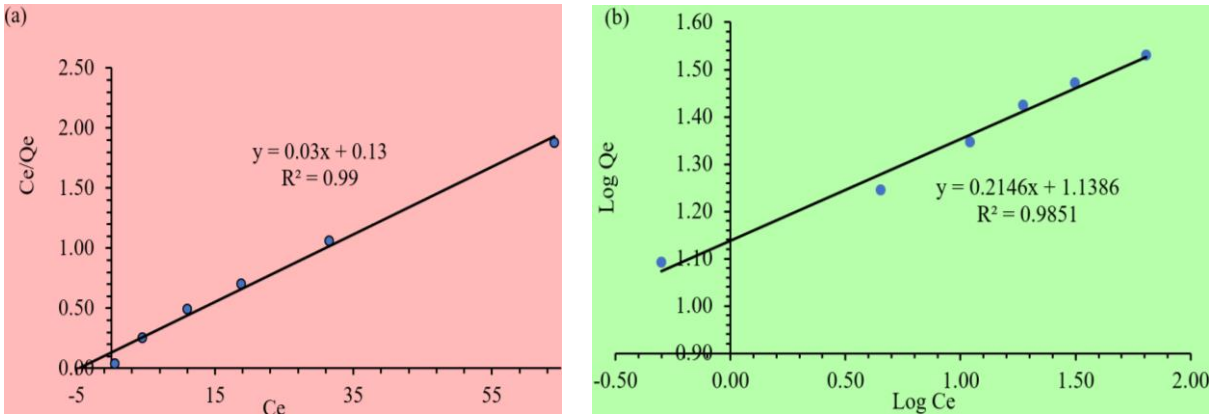

Fig. 12. Langmuir isotherm adsorption a) and Freundlich isotherm adsorption b) of MB

This shows that the production of the activated carbon from tamarind wood with NaCl and microwave activation has potential for further commercial production with a simplified process, shorter processing times, high efficiencies, a low degree of hazardous by-products, higher yields, and lower costs. The fitting of the Freundlich isotherm resulted in a high coefficient of determination as well. This indicates that MB adsorption on the TWAC was also a heterogeneous process, with van der Waals forces, hydrogen bonding, and hydrophobic interactions [33]. This corresponds well with the FTIR results (Figs. 4 and 5), which show many types of surface functional groups, dominated by carbonate, on the activated carbon product. Furthermore, a relatively low value of 1/n (0.2146) also indicates a very good or favorable adsorption process [21]. This indicated that the active sites with the highest binding energies would be used first for less heterogeneous surfaces, and then pursued by weaker sites for more heterogeneous surfaces [33]. However, the 1/n value of this isotherm is relatively low. This indicated that the binding of the MB molecule at the active sites on the TWAC has less influence on the affinity of other sites with low heterogeneity of the TWAC surface [36]. After conversion of the 1/n value to n value, the n value is in the range between 1 and 10, which also shows the favorability of the adsorption process [37]. However, the values are in middle of the range between 1 and 10, which indicates a moderately favorable adsorption process driven by physisorption [47]. In addition, a relatively high K_F value (13.759416) shows a lower free energy requirement for the adsorption process [21]. It was also indicated that the TWAC has a high adsorption capacity [39].

4. CONCLUSIONS

The percent yields (77.42-92.52%) of TWACs decreased with increasing MP from 450 W to 850 W and wt.% of NaCl from 0% to 5%. The effect of increasing wt.% of NaCl is lower than that of increasing MP, which was attributed to the formation of carbonate by NaCl. At the same time, disordered graphitic characteristics of the TWAC increased with an increase of wt.% of NaCl from 1% to 5% and MP from 450 W to 850 W. This was attributed to the acceleration of the depolymerization of aromatic structural units by NaCl to produce more volatile matters and smaller aromatic structures and heat of absorption of carbon atoms in the TWC from microwave radiation with high induction of dipole rotations. In terms of surface chemistry, the acidic surface functional groups were decomposed already with 450 W, while the basic surface functional groups remained in the TWACs until 850 W. In addition, the carbonate surface functional groups, which are the main basic surface functional groups on the TWACs, are formed by dehydration reactions and catalyzed gasification of NaCl and Na metal, respectively. However, the oxygen content of the TWACs was constant within the MP range of 600

[Downloaded from survey.iust.ac.ir on 2025-07-27]

[DOI: 10.22068/ijmse.3647]

to 850 W. This shows that the content of basic functional groups is also constant. A small content of Na and Cl elements has remained in the TWACs made with 3-5 wt.% of NaCl after the microwave treatment. This was confirmed by the investigation of morphologies by SEM, which showed some small particles on the surface of the TWACs. They also showed large tube channels, high content of small pores, rough and hard texture, and cracks on the surface of the TWACs. Investigation of the porous characteristics of the TWACs has shown that the pore widths range from 0.823 to 2.52 nm. BET surface area, pore volume, micropore, and average pore size of products have increased with increasing wt.% of NaCl and MP, but also relatively increased for activation with 3-5 wt.% NaCl and 600-850 W. The MB adsorption data of collected TWAC with 3 wt.% NaCl and 600 W showed optimum results at 60-minute equilibrium time, pH 8 maximum adsorption, and favorable Langmuir isotherm adsorption process with 96.36%-97.74% removal) with the effect of pore structure and basic surface functional groups on TWAC. These results have shown that the wt.% of NaCl and MP have an important role in the development of porous structure and surface characteristics of TWACs. This process is feasible for commercial production with low cost, short production time, high yield, and environmental friendliness.

ACKNOWLEDGEMENT

This research was partially financially supported by the Department of Chemistry, Faculty of Science, Naresuan University.

REFERENCES

[1] I.K. Tetteh, I. Issahaku, A.Y. Tetteh, “Recent advances in synthesis, characterization, and environmental applications of activated carbons and other carbon derivatives”. Carbon Trends., 2024, 14, 100328. https://doi.org/10.1016/j.cartre.2024.100328.

[2] A. Suhaimi, A.S. Abdulhameed, A.H. Jawad, T.A. Yousef, O.K. Al Duaij, Z.A. Alothman, L.D. Wilson, “Production of large surface area activated carbon from a mixture of carrot juice pulp and pomegranate peel using microwave radiation-assisted $ZnCl_2$ activation: An optimized removal process and tailored adsorption mechanism of crystal violet dye”. Diamond Relat. Mater., 2022, 130, 109456. https://doi.org/10.1016/j.diamond.2022.109456.

[3] C. Bao, A. Serrano-Lotina, M. Niu, R. Portela, Y. Li, K.H. Lim, P. Liu, W. Wang, M.A. Bañares, Q. Wang, “Microwave-associated chemistry in environmental catalysis for air pollution remediation: A review”. Chem. Eng. J., 2023, 466, 142902. https://doi.org/10.1016/j.cej.2023.142902.

[4] Z. Wu, X. Guo, Y. Liu, Y. Wang, M. Gao, C. Yao, J. Chang, H. Zhou, “Construction of porous carbon for high-performance microwave absorbing: An efficient method to utilize direct liquefaction coal asphalt by-products”. Diamond Relat. Mater., 2023, 135, 109822. https://doi.org/10.1016/j.diamond.2023.109822.

[5] T. Kim, J. Lee, K.H. Lee, “Microwave heating of carbon-based solid materials”. Carbon Lett., 2014, 15(1), 15-24. http://dx.doi.org/10.5714/CL.2014.15.1.015.

[6] R. Yang, J. Zhou, L. Wu, S. Ping, “Fabrication of developed porous carbon derived from bluecoke powder by microwave-assisted KOH activation for simulative organic wastewater treatment”. Diamond Relat. Mater., 2022, 124, 108929. https://doi.org/10.1016/j.diamond.2022.108929.

[7] É.M.L. Sousa, M. Otero, L.S. Rocha, M.V. Gil, P. Ferreira, V.I. Esteves, V. Calisto, “Multivariable optimization of activated carbon production from microwave pyrolysis of brewery wastes-application in the removal of antibiotics from water”. J. Hazard. Mater., 2022, 431, 128556. https://doi.org/10.1016/j.jhazmat.2022.128556.

[8] R.K. Liew, E. Azwar, P.N.Y. Yek, X.Y. Lim, C.K. Cheng, J.H. Ng, A. Jusoh, W.H. Lam, M.D.N.L. Ibrahim Ma, S.S. Lam, “Microwave pyrolysis with KOH/NaOH mixture activation: A new approach to produce micro-mesoporous activated carbon for textile dye adsorption”. Bioresour. Technol., 2018, 266, 1-10. https://doi.org/10.1016/j.biortech.2018.06.051.

[9] T. Phothitontimongkol, K. Prasertboonyai, “A fast removal of methyl orange from an aquatic system utilizing activated carbon from waste tamarind wood”. Desalin.

[Downloaded from survey.iust.ac.ir on 2025-07-27]

[DOI: 10.22068/ijmse.3647]

Water Treat., 2024, 317, 100267. https://doi.org/10.1016/j.dwt.2024.100267.
[10] J.N. Sahu, J. Acharya, B.C. Meikap, "Optimization of production conditions for activated carbons from tamarind wood by zinc chloride using response surface methodology". Bioresour. Technol., 2010, 101, 1974-1982. https://doi.org/10.1016/j.biortech.2009.10.031.
[11] S. Maulina, G. Handika, Irvan, A.H. Iswanto, "Quality comparison of activated carbon produced from oil palm fronds by chemical activation using sodium carbonate versus sodium chloride". J. Korean Wood Sci. Technol., 2020, 48(4), 503-512. https://doi.org/10f5658/WOOD.2020.48.4.503.
[12] A. Bahiraei, J. Behin, "Effect of citric acid and sodium chloride on characteristics of sunflower seed shell-derived activated carbon". Chem. Eng. Technol., 2021, 44(9) 1604-1617. https://doi.org/10.1002/ceat.202100117.
[13] M.I. Din, R. Khalid, Z. Hussain, S. Gul, A. Mujahid, "Synthesis and characterization of cobalt doped zinc oxide nanoparticles and their application for catalytic reduction of methylene blue dye". Desalin. Water Treat., 2024, 317, 100002. https://doi.org/10.1016/j.dwt.2024.100002.
[14] M.F.M. Yusop, M.A. Ahmad, N.A. Rosli, M.E.A. Manaf, "Adsorption of cationic methylene blue dye using microwave-assisted activated carbon derived from acacia wood: Optimization and batch studies". Arabian J. Chem., 2021, 14(6), 103122. https://doi.org/10.1016/j.arabjc.2021.103122.
[15] M.A. Mahmoud, "Kinetics and thermos-dynamics of aluminum oxide nanopowder as adsorbent for Fe(III) from aqueous solution". Beni-Suef. Univ. J. Basic Applied. Sci., 2015, 4, 142-149. https://doi.org/10.1016/j.bjbas.2015.05.008.
[16] J. Dai, F.L. Ren, C.Y. Ta, "Adsorption behavior of Fe(II) and Fe(III) ions on thiourea cross-linked chitosan with Fe(III) as template". Molecules., 2012, 17, 4388-4399. https://doi.org/10.3390/molecules17044388.
[17] L. Zhang, M. Mi, B. Li, Y. Dong, "Modification of activated carbon by means of microwave heating and its effects on the pore texture and surface chemistry". Res. J. Appl. Sci. Eng. Technol., 2013, 5(5), 1791-1795. https://doi.org/10.19026/rjaset.5.4946.
[18] D. Liu, R. Su, Z. Hao, X. Zhao, B. Jia, L. Dong, "Catalytic effect of NaCl on the improvement of the physicochemical structure of coal-based activated carbons for SO_2 adsorption". Processes., 2019, 7(6), 338. https://doi.org/10.3390/pr7060338.
[19] J. Zhu, Q. Li, Y. Che, X. Liu, C. Dong, X. Chen, C. Wang, "Effect of Na_2CO_3 on the microstructure and macroscopic properties and mechanism analysis of PVA/CMC composite film". Polymers., 2020, 12, 453. https://doi.org/10.3390/polym12020453.
[20] N. Bao, X. Miao, X. Hu, Q. Zhang, X. Jie, X. Zheng, "Novel synthesis of plasmonic Ag/AgCl@TiO_2 continues fibers with enhanced broadband photocatalytic performance". Catalysts., 2017, 7, 117. https://doi.org/10.3390/catal7040117.
[21] J. Gao, Y. Qin, T. Zhou, D. Cao, P. Xu, D. Hochstetter, Y. Wang, "Adsorption of methylene blue onto activated carbon produced from tea (Camellia sinensis L.) seed shells: Kinetics, equilibrium, and thermodynamics studies". J. Zhejiang Univ. Sci. B., 2013, 14(7), 650-658. https://doi.org/10.1631/jzus.B12a0225.
[22] M.H. Shahrokh Abadi, A. Delbari, Z. Fakoor, J. Baedi, "Effects of annealing temperature on infrared spectra of SiO_2 extracted from rice husk". J. Ceram. Sci. Tech., 2015, 6(1), 41-46. https://doi.org/10.4416/JCST2014-00028.
[23] A. Ahmadpour, H. Rashidi, M.J.D. Mahboub, M.R. Farmad, "Comparing the performance of KOH with NaOH-activated anthracites in terms of methane storage". Adsorpt. Sci. Technol., 2013, 31(8), 729-746. https://doi.org/10.1260/0263-6174.31.8.729.
[24] M. Khachani, A. El Hamidi, M. Halim, S. Arsalane, "Non-isothermal kinetic and thermodynamic studies of the dehydroxylation process of synthetic calcium hydroxide $Ca(OH)_2$". J. Mater. Environ. Sci., 2014, 5(2), 615-624.
[25] M.R. Sazegar, S. Mahmoudian, A. Mahmoudi, S. Triwahyono, A.A. Jalil, R.R. Mukti, N.H.N. Kamarudin, M.K. Ghoreishi, "Catalyzed claisen–schmidt reaction by protonated aluminate mesoporous silica nanomaterial focused on the (E)-chalcone

[Downloaded from survey.iust.ac.ir on 2025-07-27]

[DOI: 10.22068/ijmse.3647]

synthesis as a biologically active compound". RSC Adv., 2016, 6, 11023-11031. https://doi.org/10.1039/c5ra23435b.

[26] Md.H. Zahir, M.M. Rahman, K. Irshad, M.M. Rahman, "Shape-stabilized phase change materials for solar energy storage: MgO and $Mg(OH)_2$ mixed with polyethylene glycol". Nanomaterials., 2019, 9, 1773. https://doi.org/10.3390/nano9121773.

[27] H.J. Rao, "Characterization studies on adsorption of lead and cadmium using activated carbon prepared from waste tyres". Environ. Pollut. Technol., 2021, 20(2), 561-568. https://doi.org/10.46488/NEPT.2021.v20i02.012.

[28] S. Prahlada Rao, S. Sunkada, "Making sense of boiling points and melting points". Resonance., 2007, 12, 43-57. https://doi.org/10.1007/s12045-007-0059-5.

[29] Z. Zhang, H. Zhou, X. Wang, L. Zhang, P. Rao, H. Zhu, "Influence mechanism of water-soluble sodium on Zhundong coal pyrolysis". ACS Omega., 2022, 7(14), 11862-11870. https://doi.org/10.1021/acsomega.1c07311.

[30] N.H. Thang, D.S. Khang, T.D. Hai, D.T. Nga, P.D. Tuan, "Methylene blue adsorption mechanism of activated carbon synthesised from cashew nut shells". RSC Adv., 2021, 11, 26563-26570. https://doi.org/10.1039/d1ra04672a.

[31] B.B. Tanganov, "About sizes of the hydrated salt ions–the components of sea water". Eur. J. Nat. Hist., 2013, 2013(1), 36-37.

[32] Q. Zhou, X. Jiang, Y. Guo, G. Zhang, W. Jiang, An ultra-high surface area mesoporous carbon prepared by a novel MnO-templated method for highly effective adsorption of methylene blue, Chemosphere. 201 (2018) 519-529, https://doi.org/10.1016/j.chemosphere.2018.03.045.

[33] J. Fito, M. Abewaa, A. Mengistu, K. Angassa, A.D. Ambaye, W. Moyo, T. Nkambule, "Adsorption of methylene blue from textile industrial wastewater using activated carbon developed from rumex abyssinicus plant". Sci. Rep., 2023, 13, 5427. https://doi.org/10.1038/s41598-023-32341-w.

[34] H.M. El-Bery, M. Saleh, R.A. El-Gendy, M.R. Saleh, S.M. Thabet, "High adsorption capacity of phenol and methylene blue using activated carbon derived from lignocellulosic agriculture wastes". Sci. Rep., 2022, 12, 5499. https://doi.org/10.103D/s41598-022-09475-4.

[35] M.A. Franciski, E.C. Peres, M. Godinho, D. Perondi, E.L. Foletto, G.C. Collazzo, G.L. Dotto, "Development of CO_2 activated biochar from solid wastes of a beer industry and its application for methylene blue adsorption". Waste Manage., 2018, 78, 630-638. https://doi.org/10.1016/j.wasman.2018.06.040.

[36] M. Berrios, M.A. Martin, A. Martin, "Treatment of pollutants in wastewater: Adsorption of methylene blue onto olive-based activated carbon". J. Ind. Eng. Chem., 2012, 18, 780-784. https://doi.org/10.1016/j.jiec.2011.11.125.

[37] A.F. Hassan, H. Elhadidy, "Production of activated carbons from waste carpets and its application in methylene blue adsorption: Kinetic and thermodynamic studies". J. Environ. Chem. Eng., 2017, 5, 955-963. https://doi.org/10.1016/j.jece.2017.01.003.

[38] Y. Yasin, M.Z. Hussein, F.H. Ahmad, "Adsorption of methylene blue onto treated activated carbon". The Malaysian J. Anal. Sci., 2007, 11(11), 400-406.

[39] F. Marrakchi, M.J. Ahmed, W.A. Khanday, M. Asif, B.H. Hameed, "Mesoporous-activated carbon prepared from chitosan flakes via single-step sodium hydroxide activation for the adsorption of methylene blue". Int. J. Biol. Macromol., 2017, 98, 233-239. https://doi.org/10.1016/j.ijbiomac.2017.01.119.

[40] H.A. Ahsaine, M. Zbair, Z. Anfar, Y. Naciri, R. El haouti, N. El Alem, M. Ezahri, "Cationic dyes adsorption onto high surface area almond shell activated carbon: Kinetics, equilibrium isotherms and surface statistical modeling". Mater. Today Chem., 2018, 8, 121-132. https://doi.org/10.1016/j.mtchem.2018.03.004.

[41] M. Qiu, Y. Xuan, P. Luo, Z. Wang, J. Shou, "Adsorption of methylene blue by activated carbon from capsicum straw". Nat. Environ. Pollut. Technol., 2015, 14(4), 859-864.

[42] H. Cherifi, B. Fatiha, H. Salah, "Kinetic

[Downloaded from survey.iust.ac.ir on 2025-07-27]

[DOI: 10.22068/ijmse.3647]

studies on the adsorption of methylene blue onto vegetal fiber activated carbons". Appl. Surf. Sci., 2013, 282, 52-59. https://doi.org/10.1016/j.apsusc.2013.05.031.

[43] Y. Bao, G. Zhang, "Study of adsorption characteristics of methylene blue onto activated carbon made by salix psammophila". Energy Procedia., 2012, 16, 1141-1146. https://doi.org/10.1016/j.egypro.2012.01.182.

[44] Md.A. Islam, S. Sabar, A. Benhouria, W.A. Khanday, M. Asif, B.H. Hameed, "Nanoporous activated carbon prepared from karanj (Pongamia pinnata) fruit hulls for methylene blue adsorption". J. Taiwan Inst. Chem. Eng., 2017, 74, 96-104. https://doi.org/10.1016/j.jtice.2017.01.016.

[45] D.A.G. Sumalinog, S.C. Capareda, M.D.G. de Luna, "Evaluation of the effectiveness and mechanisms of acetaminophen and methylene blue dye adsorption on activated biochar derived from municipal solid wastes". J. Environ. Manage., 2018, 210, 255-262. https://doi.org/10.1016/j.jenvman.2018.01.010.

[46] J. Wang, J. Ma, Y. Sun, "Adsorption of methylene blue by coal-based activated carbon in high-salt wastewater". Water., 2022, 14(21), 3576. https://doi.org/10.3390/w14213576.

[47] S. Wong, N.A.N. Yac'cob, N. Ngadi, O. Hassan, I.M. Inuwa, "From pollutant to solution of wastewater pollution: Synthesis of activated carbon from textile sludge for dye adsorption". Chin. J. Chem. Eng., 2018, 26, 870-878. https://doi.org/10.1016/j.cjche.2017.07.015.

[48] D. Pathania, S. Sharma, P. Singh, "Removal of methylene blue by adsorption onto activated carbon developed from ficus carica bast". Arabian J. Chem., 2017, 10, S1445-S1451. http://doi.org/10.1016/j.arabjc.2013.04.021.

[49] Y. Xia, Q. Yao, W. Zhang, Y. Zhang, M. Zhao, "Comparative adsorption of methylene blue by magnetic baker's yeast and EDTAD-modified magnetic baker's yeast: Equilibrium and kinetic study". Arabian J. Chem., 2015, 12(8), 2448-2456. https://doi.org/10.1016/j.arabjc.2015.03.010.

[50] K.A.M. Said, M.A.M. Amin, I. Yakub, M.R. Rahman, A.B.H. Kueh, S. Hamdan, M.M. Rahman, "Methylene blue adsorption mechanism onto palm kernel shell-derived activated carbon: From particle diffusion to site adsorption". BioResources., 2023, 18(3), 5120-5132. https://doi.org/10.15376/biores.18.3.5120-5132.

[51] Y. Nagasawa, Y. Seida, T. Gotoh, E. Furuya, "Influence of hydrophobicity of backbone polymer in thermo-responsive hydrogel with immobilized amine on cycle capacity for absorption and recovery of CO_2". Polymers., 2019, 11, 1024. https://doi.org/10.3390/polym11061024.

[Downloaded from survey.iust.ac.ir on 2025-07-27]

[DOI: 10.22068/ijmse.3647]